

Sol–Gel-Deposited Ti-Doped ZnO: Toward Cell Fouling Transparent Conductive Oxides

Rehab Ramadan,^{†,‡} David Romera,[§] Rosalía Delgado Carrascón,[†] Miguel Cantero,[⊥] John-Jairo Aguilera-Correa,[§] Josefa P. García Ruiz,^{||} Jaime Esteban,[§] and Miguel Manso Silván^{*,†}

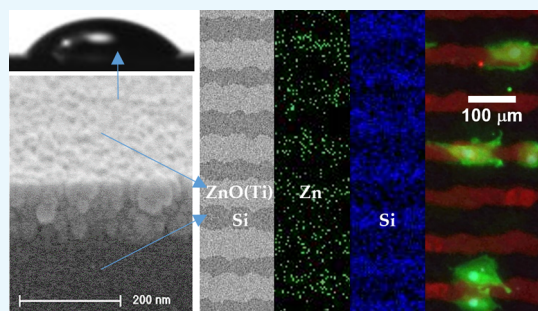
[†]Departamento de Física Aplicada and Instituto de Ciencia de Materiales Nicolás Cabrera, ^{||}Departamento de Biología Molecular, and [⊥]Departamento de Física de la Materia Condensada and Instituto de Ciencia de Materiales Nicolás Cabrera, Universidad Autónoma de Madrid, 28049 Madrid, Spain

[‡]Physics Department, Faculty of Science, Minia University, 61519 Minia, Egypt

[§]Departamento de Microbiología Clínica, Instituto de Investigación Sanitaria de la Fundación Jiménez Díaz, Av. Reyes Católicos 2, 28040 Madrid, Spain

Supporting Information

ABSTRACT: Ti-doped ZnO thin films were obtained with the aim of tailoring ZnO film bioadhesiveness and making the optoelectronic properties of ZnO materials transferable to biological environments. The films were prepared on silicon substrates by sol–gel spin-coating and subsequent annealing. A Ti–O segregation limits the ZnO crystallite growth and creates a buffer out-layer. Consequently, the Ti-doped ZnO presents slightly increased resistivity, which remains in the order of $10^{-3} \Omega\cdot\text{cm}$. The strong biochemical interference of Zn^{2+} ions released from pure ZnO surfaces was evidenced by culturing *Staphylococcus epidermidis* with and without the Zn^{2+} coupling agent clioquinol. The Ti-doped ZnO surfaces showed a considerable increase of bacterial viability with respect to pure ZnO. Cell adhesion was assayed with human mesenchymal stem cells (hMSCs). Although hMSCs find difficulties to adhere to the pure ZnO surface, they progressively expand on the surface of ZnO when the Ti doping is increased. A preliminary microdevice has been built on the Si substrate with a ZnO film doped with 5% Ti. A one-dimensional micropattern with a zigzag structure shows the preference of hMSCs for adhesion on Ti-doped ZnO with respect to Si. The induced contrast of surface tension further induces a cell polarization effect on hMSCs. It is suggested that the presence of Ti–O covalent bonding on the doped surfaces provides a much more stable ground for bioadhesion. Such fouling behavior suggests an influence of Ti doping on film bioadhesiveness and sets the starting point for the selection of optimal materials for implantable optoelectronic devices.



1. INTRODUCTION

The long trajectory of ZnO within advanced sensing and actuating structures and the oligomineral nature of the degradation product Zn^{2+} invites to applications of this material in implantable devices.¹ In fact, this material is known for its versatile properties (photostable, nontoxic, inexpensive, and abundant).² In appropriate conditions, ZnO is a transparent semiconductor presenting high conductivity with a wide spectrum of optoelectronic applications (light-emitting diodes, photodetectors, or photovoltaic cells) in which ZnO is used mostly as a transparent conductive oxide (TCO).^{3,4} ZnO doping with Al, Ga, In, Ti, Zr, and B^{5–8} has been studied to improve the ZnO performance as a TCO. Very often, the doping strategies seek high electron mobilities to provide alternative materials to In:SnO₂ (ITO).⁹ Alternatively to doping, the formation of nanocomposites allows establishing a dual electronic and optical role to ZnO-based films.¹⁰

The advances in nanotechnology are expanding the applications of ZnO to the biomedical field. Doping ZnO

with different elements is in fact useful for cellular imaging.¹¹ ZnO photoluminescent nanoparticles can be doped with Co, Cu, or Ni and stabilized in aqueous colloidal solutions.¹² Relevantly, selected ZnO nanoparticles are able to penetrate into the cell nucleus, which opens imaging possibilities and potential genotoxic activity against cancer cells.¹³ Additionally, ZnO nanomaterials are being employed in the development of drug delivery systems exploiting engineered surface chemistry and large surface areas.¹⁴ Especially, ZnO has excellent properties for biosensing, such as strong adsorption capability and high isoelectric point, which allow detection of the adsorption of certain proteins, enzymes, and antibodies.¹⁵ The synthesis of ZnO nanostructures opens its use to nonenzymatic biosensor systems¹⁶ and self-powered nanosensors.¹⁷ In other applications, ZnO nanowires have been exploited as bio-

Received: March 8, 2019

Accepted: May 17, 2019

Published: July 1, 2019

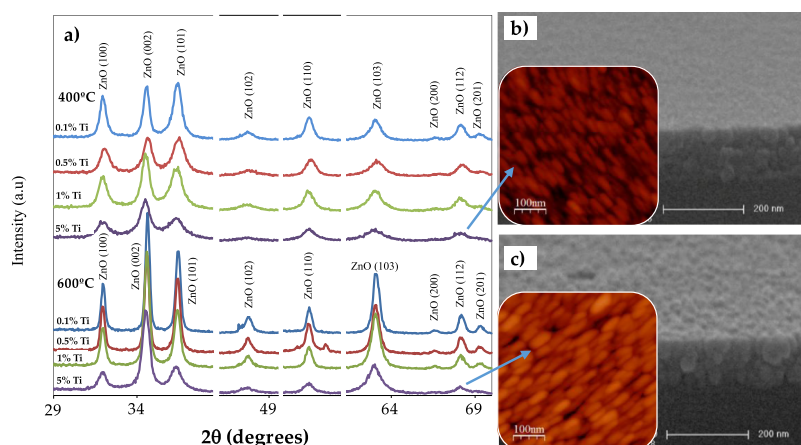


Figure 1. (a) X-ray diffractograms for ZnO:Ti films with doping levels of 0.1, 0.5, 1, and 5% Ti with respect to Zn (from top to bottom) annealed at 400 °C (top set) and 600 °C (bottom set). Miller indices according to the ZnO wurtzite phase. FE-SEM perspective view micrographs and AFM 500 × 500 nm² topography images (insets) of ZnO samples with 5% Ti after annealing at 400 (b) and 600 °C (c) (the z-scale in the AFM images is 25 nm).

medical piezoelectric devices. However, the biomedical applications of ZnO are drastically limited by its intrinsic solubility, which shortens the stability and lifetime of devices in cell culture conditions.^{18,19}

Outstandingly, the previously mentioned use of ZnO structures for self-powering devices extends the use of ZnO out of the biomedical context to the emerging field of bio-based power sources and artificial leaves. In fact, the role of TCOs in biophotovoltaic systems has been already put in relevance underlining the complexity for separation of photogenerated centers after surface immobilization.²⁰ Relevantly, a configuration of ZnO nanowires has already been proposed in a “bio-hybrid solar cell”.²¹ All these reports point to an increasing demand of ZnO-based TCOs in biological environments and to the need of a prospective materials research in bioengineered TCOs.

In this paper, we propose the synthesis of Ti-doped ZnO thin films with different Ti contents in order to regulate the surface bioadhesiveness *in vitro*. Ti oxides present a covalent character that can be used to compensate the strong ionic character of ZnO and compensate its exacerbated solubility in alkaline solutions at 37 °C. We propose that this process can be used to tune its physical properties and most relevantly its biofouling properties. The effects of Ti doping on the microstructure, surface properties, and conductivity of the films are studied in detail prior to the *in vitro* analysis of the bioadhesiveness of the surfaces at the bacterial and human cell level. To evaluate their potential for integration in biomedical devices, a microdevice application is demonstrated by applying a photolithographic sequence to selected Ti-doped ZnO films and observing the response of human mesenchymal stem cells (hMSCs).

2. RESULTS AND DISCUSSION

2.1. Microstructural Characterization. The ZnO thin films with different annealing treatments (400 and 600 °C) and Ti doping levels (from 0.1 to 5% Ti) were analyzed by X-ray diffraction (XRD). The corresponding diffractograms are presented in Figure 1a. The samples were all polycrystalline independently of the annealing temperature and doping level. All the samples fitted well the wurtzite structure, labeled with appropriate Miller indices on the diffractogram. It could be

observed that the increase of the annealing temperature has a positive effect on the growth of crystallite size, with higher intensity/width ratios for the diffraction peaks in the 600 °C annealed sample, at an equivalent doping level.

In fact, it is significant that all the ZnO:Ti thin films which have been annealed at 600 °C exhibit a dominant (002) peak, although according to the reference diffraction patterns, the (101) plane should be the most intense. Consequently, (002) appears as a preferential direction of growth and orientation of ZnO thin films. High temperatures of 600 °C further favor this preferential growth.

The best defined diffraction peaks of hexagonal ZnO correspond to the lowest Ti doping levels of 0.1%. In fact, as the Ti content increases, the diffraction peaks loose resolution and suffer a peak shift, as predicted by Vegard's law. Excess Ti induces point defects and consequently tensions within the ZnO structure in view of the coordination and lattice mismatch between the two potential final structures of a solid solution (considering wurtzite for ZnO and anatase for TiO₂). The increase of Ti % also affects the preferential growth along (002). Although low Ti % leads to a clear preferential growth [note relative intensities of (002) and (100) peaks of 4:1 for 0.1% Ti sample], this effect is drastically reduced after Ti enrichment [intensities of (002) and (100) peaks of 7:3 for 5% Ti sample].

The effect of Ti doping level and annealing temperature had a direct effect in the average crystallite size considering the preferential growth direction, as calculated by applying a Lorentzian fitting to the (002) peak and using the best fit parameters into Scherrer's formula.²² Figure S1 reveals that the mean crystallite size in the (002) preferential direction remains within the 10–40 nm range and decreases when the amount of Ti increases in the sample. Additionally, it increases with the annealing temperature of the samples.

Relevantly, this microstructural effect of doping and annealing also influences the final surface topography of the film. Figure 1b,c corresponds to field emission scanning electron microscopy (FE-SEM) cross-sectional micrographs and atomic force microscopy (AFM) surface topography images from the surfaces of ZnO doped with 5% Ti annealed at 400 and 600 °C, respectively. The films reach an overall thickness of 180 and 160 nm for 400 and 600 °C annealing,

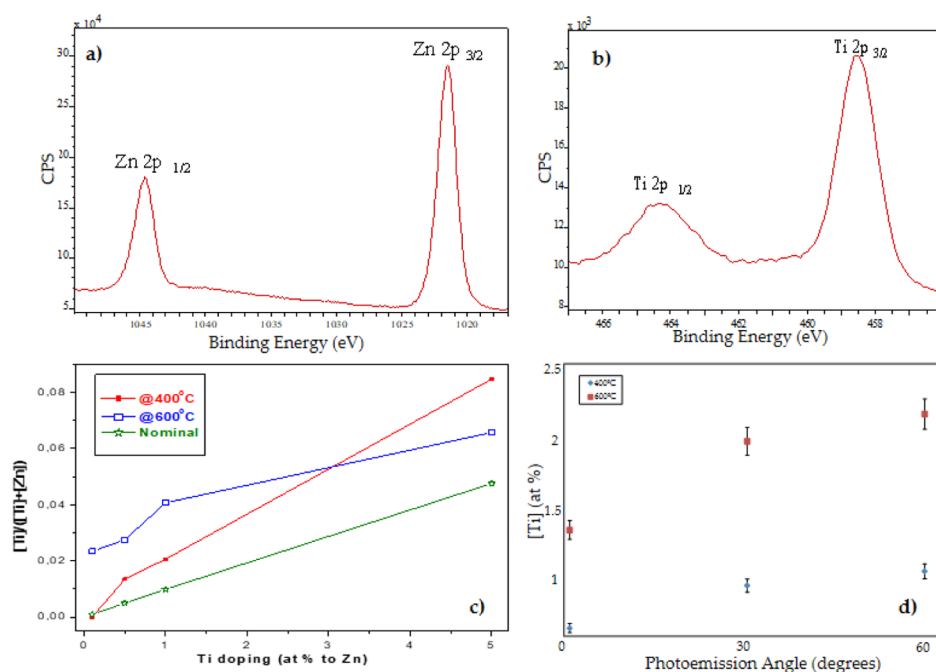


Figure 2. Characteristic Zn 2p (a) and Ti 2p (b) core-level XPS spectra of 5% Ti-doped ZnO sample annealed at 600 °C. (c) Normalized $[Ti]/([Ti] + [Zn])$ ratio calculated from the survey spectra of the ZnO samples doped at 0.1, 0.5, 1, and 5% Ti after 400 and 600 °C annealing compared with the nominal expected value (lines indicate exclusively trends). (d) Variation of Ti at. % for increasing photoemission angle for samples doped at 5% at 400 and 600 °C.

respectively, which confirms the continuous condensation effect of annealing temperature on sol–gel-deposited films. It can be noted that the mean grain size is in the same order of magnitude as the crystallite size estimated by XRD (ca. 15 and 50 nm for 400 and 600 °C annealing, respectively), confirming the effect of the annealing temperature on the microstructure. Additionally, the emphasized grain growth activated at 600 °C and the crystallite growth constrictions due to high doping level lead to an increasingly rough surface. Prominent grain heads emerge from the surface, leading to a pseudopyramidal profile. In fact, the root-mean-square roughness (R_{rms}) estimated from the AFM images clearly indicates a temperature activation of the roughness, with values of 1.2 ± 0.2 and 1.7 ± 0.1 nm for the ZnO:Ti 5% samples annealed at 400 and 600 °C, respectively. The complementary analysis of ZnO control samples further illustrated the temperature activation of the roughness. Remarkably, no significant differences were identified in the R_{rms} for films with common annealing temperature but differing in Ti doping (see Figure S2). With respect to the relevant microscopic information related to mechanics, the films show no surface-cracking and good interface adhesion, denoting the formation of a continuous relaxed film with no drastic tendency toward delamination.

2.2. Surface Composition and Wetting. Prior to a surface inspection, the in-depth analysis of the films was accomplished by Rutherford backscattering spectrometry (RBS) measurements in C resonant conditions. These analyses showed that the in-depth composition was relatively homogeneous, with some slight surface enrichment in Ti and with abundant C incorporation (ca. 10% for all the films), irrespective of the doping level of the films. Figure S3 details the experimental and analyzed spectra of ZnO:Ti 5% after annealing at 400 and 600 °C (left) and the derived in-depth analyses (right). In order to obtain a more resolved estimation of the surface composition on the top of the layers, XPS

spectra were obtained. The surfaces of ZnO:Ti thin films were composed of Zn, O, Ti, and C (plus a nonaccountable amount of H) with relative composition depending on the annealing temperature and doping level. Only the sample with a highest Ti doping level (5%) and annealed at a lower temperature (400 °C) presented a Cl residue below 1 at. %. In particular, there were no traces of Si, which confirms the conformal character of the coating on the substrate and the lack of substrate out-diffusion.

Relevantly, the chemical state of Zn and Ti was evaluated by obtaining the corresponding Zn 2p and Ti 2p core-level spectra. Figure 2a,b shows the Zn 2p and Ti 2p core-level spectra for the 5% Ti-doped ZnO surfaces after 600 °C annealing. The characteristic binding energies (BEs) of the peaks, with 3/2 splitting components at ca. 1021.5 and 458.5 eV, respectively, and their shape clearly illustrate that the chemical state corresponds to the oxidized Zn (Zn^{2+} state) and Ti (Ti^{4+} state), such as in well-formed ZnO and TiO_2 .^{23–25} The O 1s peak (not shown) can be consistently fitted by two components at 532.0 eV, which is attributed to oxygen in TiO_2 , and the one at 531.0 eV corresponding to oxygen in the ZnO structure.²⁷ The described BEs and peak ratios were common for all the analyzed ZnO:Ti samples at varying annealing temperature (400 vs 600 °C) and Ti concentration (from 0.1 to 5%).

Quantitative data obtained from the survey spectra were used to monitor the level of surface integration of Ti and Zn with respect to the nominal values used in the design of the synthesis. The results of $[Ti]/([Ti] + [Zn])$ are plotted in Figure 2c for the two annealing temperatures and a whole range of Ti doping to illustrate a clear enrichment of the surface in Ti with respect to the expected nominal value. This enrichment is generalized for all Ti doping levels and annealing temperatures (only the sample annealed at 400 °C at the lowest doping levels shows a value equal to the nominal one).

The origin of this surface enrichment can be due to both a preferential condensation of the Ti precursor during spin-coating because of the fast xerogel formation kinetics of the titanium precursor and a surface segregation of the minority element upon thermal annealing.

To further investigate this point, the surface composition was evaluated at two additional photoelectron take-off angles for the samples with the highest Ti doping level and both annealing temperatures. The results indicate an increase of Ti concentration at the increasing take-off angle, which is a clear indication of the surface segregation of Ti. Additionally, this segregation is more pronounced for the sample annealed at 600 °C, which confirms the critical role played by the annealing process in this segregation.

To understand the behavior of the surface of the ZnO films, the water contact angle (WCA) was evaluated at different doping conditions and annealing temperatures. All the surfaces exhibited a mild hydrophilic character with WCA values ranging from 55 to 85°, as illustrated in Figure 3. The effect of

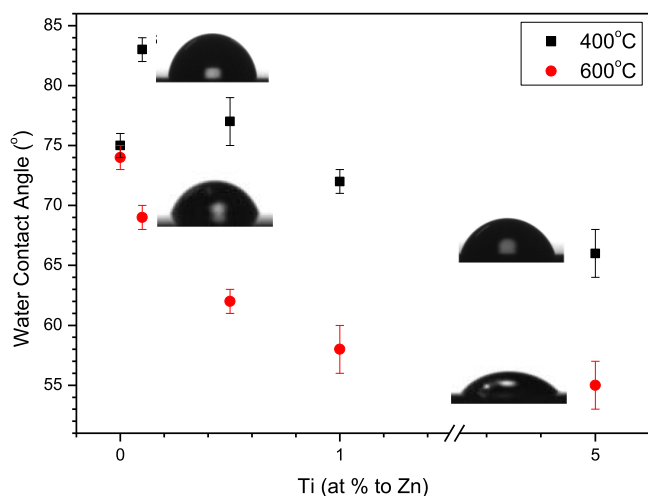


Figure 3. Variation of WCA for the samples treated at 400 °C (squares) and 600 °C (circles) and the different Ti doping from 0 (pure ZnO) to 5% Ti.

both Ti doping and annealing temperature can be derived from the image. An increasing amount of Ti in the ZnO films induced a decrease of the WCA. However, by comparing the

pure ZnO surface at 400 °C, the effect of low additions of Ti induced an increase of WCA, while this transition was to a smaller contact angle for the series annealed at 600 °C. In fact, the contact angle of pure ZnO surfaces exhibited no significant difference for the 400 and 600 °C annealed samples.

For the rest of the samples, at equivalent Ti doping, the surfaces exhibited a higher WCA at lower annealing temperatures. The overall behavior can be understood in terms of an interplay between surface chemistry and topography. An increasing TiO_x fraction induces a more hydrophilic behavior through reinforced dipolar interactions. On the other hand, the topographic effects induced by annealing at 600 °C make the surfaces more hydrophilic with respect to the equivalent at 400 °C. Such reduction of WCA for a rougher surface reinforces the idea of a strong water–surface interaction regime in agreement with the Wenzel model.²⁶

2.3. Functional Properties. For a complete analysis of the effects of the segregation of Ti to the film surface, the resistivity was measured using the van der Pauw method.²⁷ The results denoted a narrow range of surface resistivity for the series of samples annealed at 400 and 600 °C ($[1-9] \times 10^{-3}$ and $[1-5] \times 10^{-3} \Omega\text{-cm}$, respectively). However, it was not possible to establish a trend with respect to the effects of Ti doping or annealing temperature. Alternatively, Au metallic contacts were deposited through a micromask on the surfaces of pure ZnO films and those with 5% Ti doping (at both annealing temperatures) and the impedance response was analyzed.²⁸ The results are plotted in the Nyquist diagrams of Figure 4a.

Both the effects of doping and annealing show relevant influence on the final electrical properties. A simple resistor in parallel to a capacitor model (R_1 , C_1 equivalent circuit shown in the inset of Figure 4a) was observed to fit the response of all samples. The resistor can be interpreted as the direct opposition to charge transfer through the ZnO film, while the capacitor appears as a contribution of the accumulation of charge, mainly in grain boundaries and contact to sample interface.

Relevantly, the presence of Ti doping induces a considerable increase of the equivalent resistance and a decrease of the capacitor value, irrespective of the annealing temperature considered. This can be explained in terms of the microstructural/surface effects observed upon doping and annealing of ZnO films. In fact, the described tendency is compatible with the formation of a Ti–O-based grain boundary on the

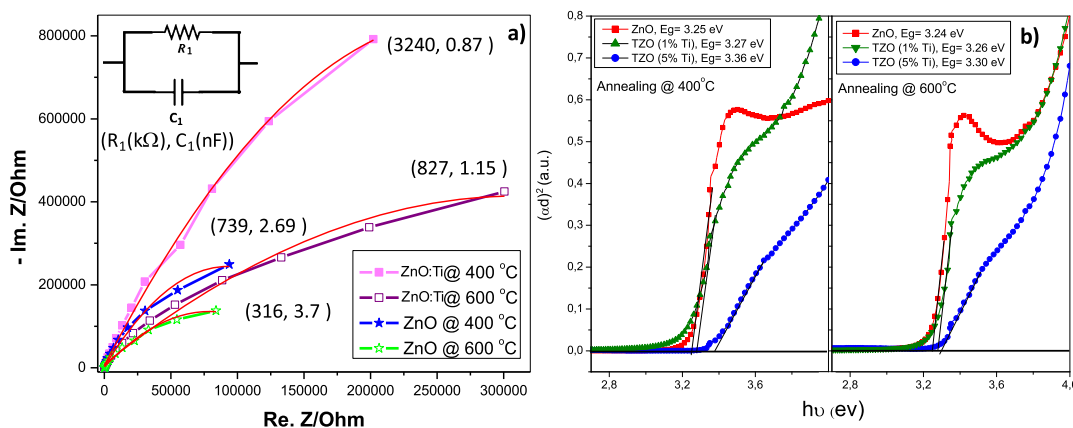


Figure 4. (a) Nyquist diagrams and impedance analysis corresponding to pure and 5% doped ZnO films after annealing at 400 and 600 °C. (b) Tauc plots for ZnO, ZnO:Ti 1%, and ZnO:Ti 5% after annealing at 400 °C (left) and 600 °C (right).

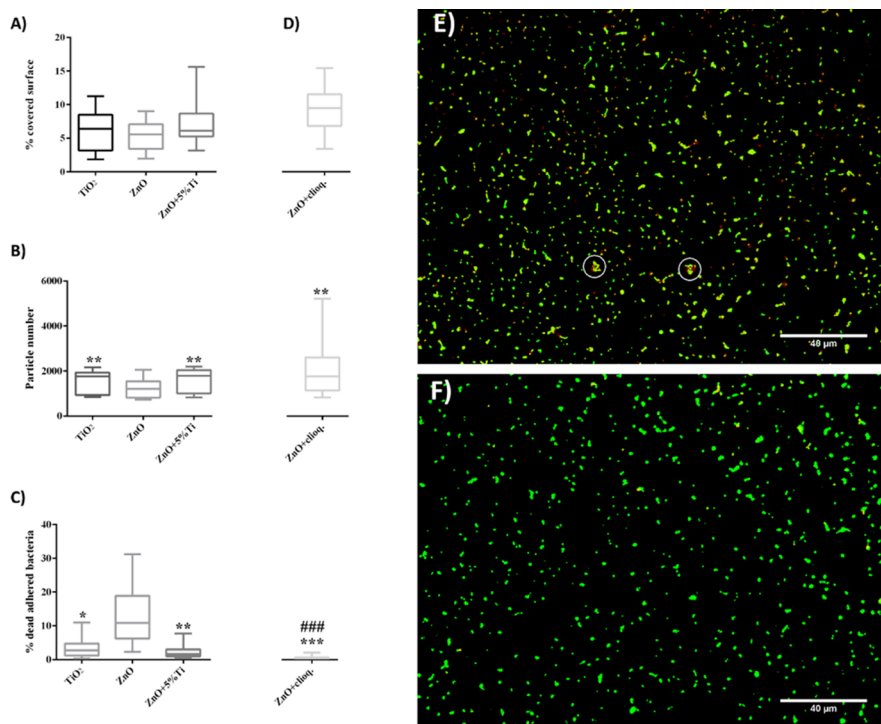


Figure 5. (a) Area of adhesion (% coverage) of *S. epidermidis* on the surfaces of ZnO doped with 5% Ti (annealed at 600 °C) compared with controls for pure ZnO and TiO₂. (b) Particle counting on the same surfaces. (c) Viability (% of dead adhered bacteria) on the same surfaces. (d) Comparison of the previous parameters on the ZnO surface in the presence of cloquinol. Fluorescence microscopy images of *S. epidermidis* adhered on the surface of ZnO without (e) and with (f) addition of cloquinol. ####: p -value < 0.0001 for Wilcoxon test compared to TiO₂. *: p -value < 0.05 for Wilcoxon test compared to ZnO. **: p -value < 0.01 for Wilcoxon test compared to ZnO. ***: p -value < 0.001 for Wilcoxon test compared to ZnO.

ZnO nanocrystals, and with the consequent promotion of a surface conduction deactivating charge accumulation in grain boundaries. These effects were, however, milder for the samples annealed at 600 °C, suggesting that grain growth has a dominant effect on favoring film conduction over the potential negative effects of surface segregation of a Ti–O-rich surface.

The effects of Ti doping on the optical properties of the films are illustrated in Figure 4b for a ZnO reference and ZnO films doped with 1 and 5% Ti. The results are illustrated in the form of Tauc plots obtained from UV–vis spectra, which reflected no characteristic absorption bands (uncolored films). Relevantly, the Tauc plots visibly illustrate the increasing spectral range induced by Ti doping. Although the optical band gap for our sol–gel reference ZnO annealed at 400 °C is 3.25 eV, this band gap is slightly widened to 3.27 eV with 1% Ti doping and up to 3.36 eV for 5% Ti-doped samples, Figure 4b (left). The main effect of the annealing at 600 °C is a slight reduction of the optical band gap, which can be correlated with the microstructural information that confirms the increase of crystallite size at this temperature. The increase of the optical band gap upon Ti doping is also related to the microstructure. In fact, the inhibition of grain growth with doping allows maintaining a crystallite size within the nanoscale, which conditions a band gap widening in ZnO materials.²⁹

2.4. Cell Adhesion. The behavior of the Ti-doped films was assayed at two different levels. We initially explored the interaction of the surfaces with bacteria. In order to limit the number of samples, the properties derived from the microstructural and physical properties was used to screen most relevant samples. To make the Ti surface segregation effects

patent on the surfaces, adhesion assays with *Staphylococcus epidermidis* were performed on ZnO films doped with 5% Ti and annealed at 600 °C in comparison with references for pure ZnO and TiO₂ samples prepared from the same precursors. We evaluated the total surface covered by adhered bacteria, the number of adhered bacterial particles on the different films, as well as the bacterial viability. The results are plotted in Figure 5.

The percentage of area covered by bacteria was the same for the three types of materials (p value = 0.1218 for Kruskal–Wallis test, Figure 5a). We found, however, at least 4.4 times more dead adhered bacteria over ZnO films with respect to Ti-containing films (11.89%, p value < 0.05 for Wilcoxon test) (Figure 5c). It has been previously described that adherence of *S. epidermidis* to abiotic surfaces is a sequential process that involves the initial adhesion mediated by autolysins and hydrophobic interactions that evolves into irreversible adherence through the action of specialized adhesins.^{30,31} Once adhered, other molecules such as aggregation-associated protein (aap) mediate bacterial accumulation, in order to start the development of a biofilm.³² In this work, molecules involved in adherence and accumulation are already expressed on the surface of the bacteria and explains the similar surface coverage observed on all the surfaces shown in Figure 5a. However, by the relatively short time of 90 min, defined by the observation of a high percentage of dead bacteria on ZnO surfaces, *S. epidermidis* has not been able to form a stable biofilm. The bactericidal behavior on ZnO is consistent with previously published literature that shows the intrinsic toxicity of ZnO due to the release of Zn²⁺ ions, which destabilize the ionic environment of the bacterial membranes.^{33,34} We did

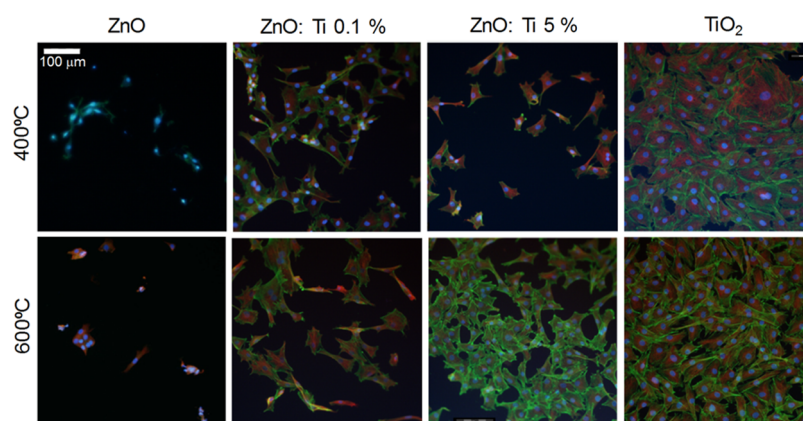


Figure 6. hMSCs cultured on the surface of the ZnO:Ti films annealed at 400 (top) and 600 °C (bottom) and different doping levels (from left to right: ZnO, ZnO:Ti 0.1%, ZnO:Ti 5%, and TiO₂). Green, actin cytoskeleton/red, α -catenin intermediate fibers/blue, DAPI nuclear staining.

additional analyses to bacterial viability by reversing the effect of Zn²⁺ ions by using the chelating agent clioquinol. In this case, the viability increased considerably, overpassing that of the surfaces containing Ti (Figure 5d).

Additionally, although the bacterial coverage of the samples was essentially the same, we found that particle counting was significantly lower when bacteria were grown on ZnO films than on the other materials (p value < 0.001), showing 31% less counts (Figure 5b). This effect on pure ZnO is potentially a consequence of the release of Zn²⁺ ions to the solution from the material. In fact, Zn²⁺ favors the aap action, present on the surface of *S. epidermidis*,³⁵ causing the higher aggregation in small groups of adhered bacteria on ZnO films, which include both live and dead ones (Figure 5e,f).

We also performed the analysis of bacterial viability by using clioquinol, obtaining a high viability (97–99%) (p value = 0.0811) on the pure ZnO samples with respect to the Ti-doped and TiO₂ controls (compare the second column in Figure 5c with the last column corresponding to clioquinol experiments shown in Figure 5d). Figure 5e,d illustrates the response of *S. epidermidis* adherence on the pure ZnO surfaces, denoting aggregation and cell death on pure ZnO films (Figure 5e), which can be chemically reversed by dosing clioquinol (Figure 5d). These results suggest that the ZnO films release zinc ions in solution, whereas the addition of 5% of Ti displays similar features to the TiO₂ surface when testing bacterial adhesion and viability.

In order to evaluate the interaction of human cells with the ZnO:Ti films, hMSCs were cultured on surfaces with different doping levels and annealing temperatures. The analysis was performed in this case for samples with minimum and maximum Ti doping (0.1 and 5% Ti) and both annealing temperatures (400 and 600 °C) taking pure ZnO and TiO₂ films as controls. The surface–material interaction was evaluated from fluorescence microscopy images obtained after 72 h of culture. Figure 6 shows the typical response of hMSCs to the different surfaces. It can be observed that cells cultured on ZnO (irrespective of annealing temperature) exhibit retracted actin cytoskeleton and intermediate catenin fibers, denoting difficulties for the progression of focal adhesions. In these conditions, cells aggregate and show a preference for cell–cell interactions rather than for cell–surface interactions. A drastic change in the interaction is observed upon integration of the smaller amount of Ti. In fact, cells spread considerably, develop polygonal shape, and exhibit

elongated filopodia, suggesting some ease for the formation of focal adhesions with respect to pure ZnO surfaces. The cells tend to keep physically interconnected but leave voids in between them in contrast with the previous behavior on pure ZnO. This tendency is reinforced when the level of Ti doping is increased to 5% and an annealing is performed at 600 °C. No drastic change is observed between the two Ti doping levels for annealing temperatures of 400 °C. Relevantly, the increase of cell spreading and total surface coverage observed on samples with 5% Ti doping and 600 °C annealing is comparable with the one observed on the TiO₂ controls. This result is in agreement with the protective character of TiO₂-coated materials and their ability to induce cell adhesion.³⁶

To establish a more quantitative evaluation of these data, we performed a morphometric analysis based on four frames of three different samples for each type of surface. The cell spreading can be considered as an indirect measurement of availability of cell binding sites on the films. However, in local environments with high cell density, cell spreading may be affected by competitive processes among the cells. The results of cell expansion area are shown in the histogram of Figure 7. In spite of the wide error bars, these data significantly illustrate the tendency of cells to favorably spread on Ti-doped surfaces, irrespective of the annealing temperature of the films.

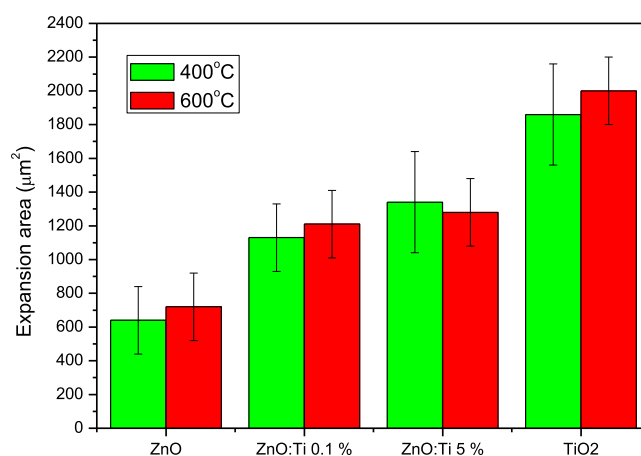


Figure 7. Expansion area of hMSCs cultured on the surface of pure ZnO, ZnO:Ti 0.1 at. %, ZnO:Ti 5 at. %, and TiO₂ after annealing at 400 and 600 °C.

The combined information obtained from the culture of bacteria and hMSCs points to an influence of ZnO solubility on the bioadhesion through an interaction with Zn^{2+} ions. However, the presence of TiO bonds, much more covalent than dominantly ionic bonds in ZnO, can determine a much more stable ground for biomolecular adsorption, a starting point in the process of cellular fouling to surfaces. Although the control of surface charge is a main aspect influencing ionic interactions with proteins and favoring protein adsorption, the phenomenon is jeopardized if the environment induces a loss of cohesive forces in the substrate material. Thus, the surface is no longer able to sustain electrostatic interactions with foreign bodies, such as proteins, being involved in a self-disruption.³⁷

In order to assess the bioadhesiveness of the ZnO:Ti films in a microdevice application, hMSCs were cultured on the surfaces of one-dimensional (1D) zigzag micropatterns on silicon substrates. For this experiment, the surfaces of ZnO doped with 5% Ti and annealing at 600 °C were chosen. The structure of the zigzag micropattern can be identified in the SEM image of Figure 8a, showing the Si/ZnO:Ti parallel lines

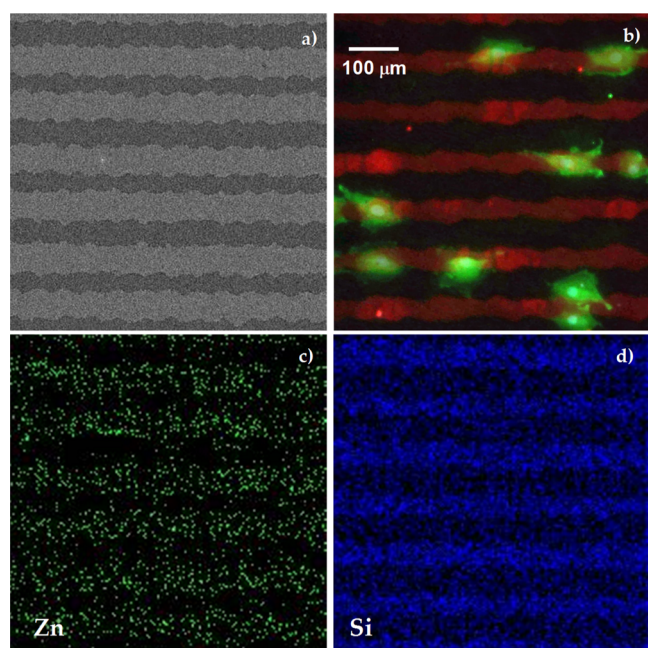


Figure 8. (a) SEM image of a ZnO:Ti/Si zigzag 1D micropattern grown with 5% Ti and annealing at 600 °C. (b) hMSCs cultured on the surface of ZnO:Ti/Si zigzag 1D micropattern (green, actin cytoskeleton/red, magnified ZnO:Ti self-fluorescence/blue, DAPI nuclear staining). (c,d) EDS complementary maps of Zn and Si, respectively.

with variable coarsening. The fluorescence microscopy results (see Figure 8b) show that, in spite of the zigzag effects, hMSCs perceive the surface of the ZnO:Ti structures as attractive for adhesion, instead of the previously illustrated and reported poor adhesion on pure ZnO.

Relevantly, the cells stand preferentially on ZnO:Ti areas rather than on Si and exhibit polarization along the main axis of the 1D ZnO:Ti structures, as illustrated by the energy-dispersive spectroscopy (EDS) maps of Zn and Si (Figure 8c,d, respectively). We underline that this selective adhesion must result from the perception of a surface-free energy contrast by hMSCs. Our contrasts have clear topographic and chemical contrasts (flat Si vs nanorough ZnO:Ti), which may

cooperatively contribute to the observed adhesion selectivity. These results point to the possibility of performing new biomedical devices incorporating transition-metal oxide conductive systems with appropriate surface designs making compatible a good degree of bioadhesiveness in culture conditions and appropriate physical properties such as electrical conductivity.

3. CONCLUSIONS

Sol–gel spin-coating allows to controllably synthesize the Ti-doped ZnO thin films on silicon substrates. The final microstructure of the films depends on the level of Ti doping and on the annealing temperature. Increase of grain size and preferential growth along the *z* axis of the ZnO wurtzite structure are favored by a high annealing temperature (600 °C) and low doping levels. Additionally, the different coordination existing between ZnO and TiO₂ leads to films enriched on Ti at surface level, especially when the Ti point defect density increases because of high doping levels. The effect can be partially induced by the heterogeneous condensation during xerogel formation but is also a result of Ti surface segregation for samples with high Ti doping levels (5%) and after annealing at high temperatures (600 °C).

The modification of the surface composition and topography inherently affects the wettability of the surfaces. Samples sintered at low temperature and with low levels of Ti doping are less hydrophilic, although this hydrophilicity is mild with WCAs over 55 °C on any sample. The surface electrical properties were affected by Ti doping, with an increase of surface resistivity to values in the 10^{−3} Ω·cm range related to Ti doping, 1 order of magnitude higher than values obtained for reference ZnO-based TCO films.³⁸ Through impedance measurements, we could confirm that the annealing at 600 °C allows improving the surface electrical resistance for films doped at 5% with respect to those annealed at 400 °C. Because of the inhibition of grain growth, the ZnO:Ti films remain transparent in the whole visible spectrum and exhibit an increase of the band gap with respect to pure ZnO films obtained with equivalent deposition/annealing process.

The response of *S. epidermidis* to culture on ZnO surfaces evidences that the intrinsic release of Zn^{2+} ions has an effect in the bacterial viability and expansion on pure ZnO. This effect can be reverted by adding the Zn^{2+} chelating agent clioquinol, which underlines the role of the ionic species in the determination of the fate of the bacterial cells. Relevantly, the ZnO:Ti and TiO₂ surfaces are also able to reverse the ionic damage, which suggests that the Ti doping level of 5% is highly efficient in providing a stable ground for cell bacterial adherence.

The adhesion of hMSCs on ZnO:Ti samples has been evaluated in comparison with ZnO and TiO₂ controls. The cells adhere and increasingly expand over the surface of ZnO:Ti samples in agreement with a higher Ti doping level. The most attractive response in terms of the number of adhered cells and cell expansion is obtained for ZnO:Ti 5% after annealing at 600 °C. These conditions were used to create a basic microdevice consisting of 1D zigzag stripes. The created 1D micropattern exhibits preferential adhesion of hMSCs with respect to the Si substrate and is observed to induce cell polarization after 72 h of culture.

These results confirm that the formation of Ti-doped ZnO films is a reliable route for the fabrication of TCO thin films retaining a good degree of bioadhesiveness. This allows cell

expansion and keeps relevant physical properties such as conductivity, which are crucial for the development of new optoelectronic biodevices, such as for sensing or energy harvesting, which will require programmable lifetimes.

4. EXPERIMENTAL SECTION

4.1. Materials Processing. A solution of zinc acetate in ethanol was prepared in concentration 0.2 M. Ethanolamine was added to the solution as a chelating agent, which allows the control of the gelation and also avoids the premature linking between metallic centers. The mixture was under reflux (30–40 °C) and magnetic stirring.^{10,39} After 8 h, zinc acetate was completely dissolved and stabilized in the ethanol solution. Titanium isopropoxide ($\text{Ti}[\text{OCH}(\text{CH}_3)_2]_4$) was dissolved in ethanol in 0.2 M concentration. HCl (115 μL) was added to the solution to induce an acid catalysis.⁴⁰

Several sols were prepared to obtain different Ti concentrations. The doping level of Ti ranged from 0.1 to 5% of Zn concentration. For labeling purposes, the samples identified with “ZnO:Ti n %” refer to a ZnO thin film with n % Ti doping. Si substrates with (1 0 0) orientation were used after cleaned with ethanol and dried in N_2 flow. The sol (50 μL) was cast on the Si surface while spinning at 2500 rpm. After 40 s, the first xerogel film was formed upon solvent evaporation. Annealing treatment was applied at temperatures 400 and 600 °C to form a dense polycrystalline film. The spin-coating–annealing sequence was applied until six cumulative layers had been deposited.

For the fabrication of the micropatterned ZnO:Ti, ZnO:Ti 5% films were used after annealing at 600 °C in a process illustrated in Figure S3. A positive photoresist (Ariston-20 series) was deposited by spin-coating on the ZnO:Ti film (spin time 25 s, spin speed 4000 rpm) and then dried on a hot plate at 70 °C for 15 min (Figure S3, 1–3). The photoresist/film stack was then exposed through an acetate slide printed mask to UV radiation for 3 min (Hamamatsu LC-L1 UV-LED spot light source, 1 $\text{W}\cdot\text{cm}^{-2}$) (Figure S3, 4). The photoresist micropattern was then developed by immersing the sample in 0.35 M NaOH solution for 2 min (Figure S3, 5). The ZnO:Ti film was then sacrificed in a HF/HNO_3 (2:2) solution for 1 min, adapting recipes for wet etching of other Ti-containing sol–gel compounds (Figure S3, 6).⁴¹ The photoresist was finally lift-off in acetone and the remaining micropattern was cleaned in ethanol and distilled water (Figure S3, 7).

4.2. Materials Characterization. The crystallinity and crystal orientation of the samples were identified by XRD with $\text{Cu K}\alpha$ ($\lambda = 1.54056 \text{ \AA}$) radiation using a Siemens D5000 HR diffractometer. The intensity was determined in the $20^\circ < \theta < 70^\circ$ range in glazing angle configuration (0.5°). The morphology and thickness of the Ti:ZnO films were studied by FE-SEM in a Philips XL-40FEG operated at 10 kV on cross-sectional samples with no metallization coating. Additional SEM imaging and elementary maps on micropatterned samples were obtained with a Hitachi S-3000N equipped with an INCAx-sight EDX system from Oxford Instruments. AFM was used to monitor the differences in surface roughness of the ZnO substrates. The AFM used for these experiments was a Nanotec Electrónica (Madrid, Spain). All images were collected with rectangular Pyrex-Nitride AFM probes with Cr/Au coating and spring constant of 0.23 N/m and resonance frequency of 12, 64 kHz (PNP-DB-50, NanoWorld, Innovative Technologies, Neuchâtel, Switzerland). Images were processed by the WSxM software 5.0 develop 9.0.⁴² AFM images were

collected with 512 points in contact mode. Roughness analysis was determined by the R_{rms} .

The elemental composition and chemical bonding of the ZnO:Ti thin films was analyzed by X-ray photoelectron spectroscopy in a SPECS PHOIBOS 150 9MCD. A monochromatic Al X-ray source non-Focus-200W-12kV was employed. The survey and core-level spectra were obtained for each sample with a pass energy of 75 and 25 eV, respectively. The spectra were analyzed using CASA XPS software. RBS was used to determine the in-depth elemental composition of ZnO:Ti films including Zn, O, Ti, and C. The incident ions were 4He with an energy of 4.26 MeV to induce C resonant conditions, which drastically increase the detection sensitivity to this impurity. For spectra simulation, we used SIMNRA software⁴³ and experimental cross sections for non-Rutherford scattering from C.⁴⁴

Resistivity was measured using a four-point station applying van der Pauw's method.²⁷ Additionally, the electrical properties of the Ti-doped ZnO films were studied by electrochemical impedance spectroscopy using a Bio-Logic SP-150 system after deposition of Au surface contacts. Data acquisition was performed in a Faraday cage between two surface electrodes up to 1 kHz frequency applying a 0.5 V amplitude signal. Fitting of data to equivalent circuits was performed using the EC-Lab software (Bio-Logic Instruments). Static WCA measurements were carried out in a KSW 100 with droplet volumes of 3 μL . Results are shown as the mean value of five droplets deposited on the different ZnO:Ti films.

4.3. In Vitro Evaluation. A *S. epidermidis* ATCC 35984 strain adherence study was performed using a modified protocol described by Kinnari et al.⁴⁵ Briefly, bacteria were suspended and diluted in 0.9% NaCl saline solution (SS) (B. Braun, Melsungen, Germany), reaching 10^8 colony-forming units (cfu)/mL bacterial solution, and 5 mL of this solution was incubated onto the samples in a sterile nontreated six-well plate (Thermo Fisher Scientific, Massachusetts, USA) at 37 °C for 90 min in order to allow adhesion in a static model. These experimental conditions favor the bacteria/metal oxide interaction.⁴⁶ After incubation, the samples were washed three times with SS to remove the unattached bacteria. The samples were then stained with the Live/Dead BacLight bacterial viability kit (Thermo Fisher Scientific, Massachusetts, USA) and rinsed with sterile water.⁴⁷ Ten photographs (40 \times magnification) were taken in a DM 2000 fluorescence microscope (Leica Microsystems, Wetzlar, Germany) for each sample. The percentage of the total surface with adhered bacteria and the percentages of dead and live bacteria were calculated and analyzed by using ImageJ software. The effect of the Zn^{2+} cation was chelated by clioquinol at 1% (Sigma-Aldrich, Missouri, USA). Each experiment was performed in triplicate. Statistical analysis was performed by pairwise comparisons using the nonparametric Wilcoxon test and by nonparametric Kruskal–Wallis test for more than two groups, with a level of statistical significance of $p < 0.05$ using StataCorp software. Values are cited and represented as medians.

hMSCs were used as they are progenitors of osteochondral and adipose tissues, which allow providing a more generalized bioadhesiveness evaluation than other specialized lineages. hMSCs from healthy donors were provided by Hospital Universitario La Princesa (Madrid, Spain). Their use for research was approved by the ethical committee of the hospital upon informed consent from the donors. ZnO:Ti surfaces were

sterilized in UV, washed with phosphate-buffered saline (PBS), and seeded with 15×10^3 cells. hMSCs were incubated for 72 h (DMEM-LG adjusted to 10% fetal bovine serum) at 37 °C in 5% CO₂. After culture, hMSCs were washed with PBS and fixed with 3.7% formaldehyde in PBS. For immune staining, cells were permeated in 0.5% Triton X-100 (CSK buffer; 100 mM NaCl, 10 mM pipes pH 6.8, 3 mM MgCl₂, 3 mM EGTA, and 0.3 M sucrose). The samples were blocked with 1% bovine serum albumin in PBS. Primary reactions took place with sera from autoimmune mice. After washing, the surfaces were incubated in dark conditions with 4',6-diamidino-2-phenylindole (DAPI) (1:5000, Calbiochem), actin (green), and α -catenin (red) secondary antibodies. The surfaces were washed, dehydrated with absolute ethanol (Merck), and mounted with Mowiol/Dabco (Calbiochem). hMSCs were visualized in a fluorescence inverted microscope (Olympus IX81) coupled with a charge-coupled device color camera and analyzed using ImageJ.

■ ASSOCIATED CONTENT

● Supporting Information

The Supporting Information is available free of charge on the ACS Publications website at DOI: 10.1021/acsomega.9b00646.

Evolution of crystallite size as a function of Ti doping for annealing temperatures of 400 and 600 °C, characterization of the films by C-resonant RBS, and (c) detailed scheme of micropattern formation on ZnO:Ti (PDF)

■ AUTHOR INFORMATION

Corresponding Author

*E-mail: miguel.manso@uam.es.

ORCID

Rehab Ramadan: 0000-0002-2479-0671

Miguel Manso Silván: 0000-0002-5063-1607

Notes

The authors declare no competing financial interest.

■ ACKNOWLEDGMENTS

Funding was received through grants CTQ2017-84309-C2-2-R from Ministerio de Ciencia, Innovación y Universidades and NanoNeuroDev 2017/EEUU/11 from Santander-Universidad.

■ REFERENCES

- (1) Zhang, Y.; Nayak, T.; Hong, H.; Cai, W. Biomedical Applications of Zinc Oxide Nanomaterials. *Curr. Mol. Med.* **2013**, *13*, 1633–1645.
- (2) Jeong, W.-J.; Park, G.-C. Electrical and optical properties of ZnO thin film as a function of deposition parameters. *Sol. Energy Mater. Sol. Cells* **2001**, *65*, 37–45.
- (3) Chen, P. H.; Chen, Y. A.; Chang, L. C.; Lai, W. C.; Kuo, C. H. Low operation voltage of GaN-based LEDs with Al-doped ZnO upper contact directly on p-type GaN without insert layer. *Solid-State Electron.* **2015**, *109*, 29–32.
- (4) Hussain, B.; Ebong, A.; Ferguson, I. Zinc oxide as an active n-layer and antireflection coating for silicon based heterojunction solar cell. *Sol. Energy Mater. Sol. Cells* **2015**, *139*, 95–100.
- (5) Shirahata, T.; Kawaharamura, T.; Fujita, S.; Orita, H. Transparent conductive zinc-oxide-based films grown at low temperature by mist chemical vapor deposition. *Thin Solid Films* **2015**, *597*, 30–38.
- (6) Yang, J.; Huang, J.; Ji, H.; Tang, K.; Zhang, L.; Ren, B.; Cao, M.; Wang, L. Effect of RF power and substrate temperature on the properties of boron and gallium co-doped ZnO films. *Mater. Sci. Semicond. Process.* **2016**, *53*, 84–88.
- (7) Zhang, Y.; Zhang, X.; Zhang, X.; Wang, Y.; Dong, J.; Huang, L.; Zhang, S.; Han, D.; Cui, G.; Cong, Y. Sn-doped ZnO thin-film transistors with AZO, TZO and Al heterojunction source/drain contacts. *Electron. Lett.* **2016**, *52*, 302–304.
- (8) Caretti, I.; Yuste, M.; Torres, R.; Sánchez, O.; Jiménez, I.; Escobar Galindo, R. Coordination chemistry of titanium and zinc in Ti(1-x)Zn_{2x}O₂ (0 ≤ x ≤ 1) ultrathin films grown by DC reactive magnetron sputtering. *RSC Adv.* **2012**, *2*, 2696–2699.
- (9) Farid, S.; Mukherjee, S.; Sarkar, K.; Mazouchi, M.; Stroschio, M. A.; Dutta, M. Enhanced optical properties due to indium incorporation in zinc oxide nanowires. *Appl. Phys. Lett.* **2016**, *108*, 021106.
- (10) Gallach, D.; Le Brizoul, L.; Gautier, N.; Ynsa, M. D.; Costa, V. T.; Ceccone, G.; Landesman, J. P.; Silván, M. M. Microstructure based optical modeling of ZnO-porous silicon permeated nanocomposites. *J. Phys. D: Appl. Phys.* **2015**, *48*, 295102.
- (11) Xiong, H.-M.; Xu, Y.; Ren, Q.-G.; Xia, Y.-Y. Stable aqueous ZnO@polymer core-shell nanoparticles with tunable photoluminescence and their application in cell imaging. *J. Am. Chem. Soc.* **2008**, *130*, 7522–7523.
- (12) Stein, A.; Schroden, R. C. Colloidal crystal templating of three-dimensionally ordered macroporous solids: materials for photonics and beyond. *Curr. Opin. Solid State Mater. Sci.* **2001**, *5*, 553–564.
- (13) Gilbert, B.; Fakra, S. C.; Xia, T.; Pokhrel, S.; Mädler, L.; Nel, A. E. The Fate of ZnO Nanoparticles Administered to Human Bronchial Epithelial Cells. *ACS Nano* **2012**, *6*, 4921–4930.
- (14) Muhammad, F.; Guo, M.; Guo, Y.; Qi, W.; Qu, F.; Sun, F.; Zhao, H.; Zhu, G. Acid degradable ZnO quantum dots as a platform for targeted delivery of an anticancer drug. *J. Mater. Chem.* **2011**, *21*, 13406–13412.
- (15) Singh, S. P.; Arya, S. K.; Pandey, P.; Malhotra, B. D.; Saha, S.; Sreenivas, K.; Gupta, V. Cholesterol biosensor based on rf sputtered zinc oxide nanoporous thin film. *Appl. Phys. Lett.* **2007**, *91*, 063901.
- (16) Qi, J.; Zhang, H.; Ji, Z.; Xu, M.; Zhang, Y. ZnO nano-array-based EGFET biosensor for glucose detection. *Appl. Phys. A: Mater. Sci. Process.* **2015**, *119*, 807–811.
- (17) You, J.; Jang, K.; Lee, S.; Bang, D.; Haam, S.; Choi, C.-H.; Park, J.; Na, S. Label-free detection of zinc oxide nanowire using a graphene wrapping method. *Biosens. Bioelectron.* **2015**, *68*, 481–486.
- (18) Franklin, N. M.; Rogers, N. J.; Apte, S. C.; Batley, G. E.; Gadd, G. E.; Casey, P. S. Comparative toxicity of nanoparticulate ZnO, bulk ZnO, and ZnCl₂ to a freshwater microalga (*Pseudokirchneriella subcapitata*): The importance of particle solubility. *Environ. Sci. Technol.* **2007**, *41*, 8484–8490.
- (19) Carrascón, R. D.; Pérez, D. G.; Ruiz, J. P. C.; Silván, M. M. Compared Biocompatibility of ZnTiO₃, ZnO and TiO₂ Sol-Gel Films with Human Mesenchymal Stem Cells. *MRS Adv.* **2016**, *1*, 737–742.
- (20) Szewczyk, S.; Giera, W.; D'Haene, S.; van Grondelle, R.; Gibasiewicz, K. Comparison of excitation energy transfer in cyanobacterial photosystem I in solution and immobilized on conducting glass. *Photosynth. Res.* **2017**, *132*, 111–126.
- (21) Yaghoubi, H.; Schaefer, M.; Yaghoubi, S.; Jun, D.; Schlaf, R.; Beatty, J. T.; Takshi, A. A ZnO nanowire bio-hybrid solar cell. *Nanotechnology* **2017**, *28*, 054006.
- (22) Patterson, A. L. The Scherrer formula for x-ray particle size determination. *Phys. Rev.* **1939**, *56*, 978–982.
- (23) Wagner, C. D.; Riggs, W. M.; Davis, L. E.; Moulder, J. F.; Muilenberg, G. E. *Handbook of X-ray Photoelectron Spectroscopy*; Eden Prairie: Minnesota, 1979.
- (24) Zhong, Z. Y.; Zhang, T. Microstructure and optoelectronic properties of titanium-doped ZnO thin films prepared by magnetron sputtering. *Mater. Lett.* **2013**, *96*, 237–239.
- (25) Wang, X.; Zhang, F.; Zheng, Z.; Chen, L.; Wang, H.; Li, C.; Lui, X. Chemical composition and structure of titanium oxide films deposited on LTI-carbon by IBED. *Thin Solid Films* **2000**, *365*, 94–98.

- (26) Wenzel, R. N. Resistance of solid surfaces to wetting by water. *Ind. Eng. Chem.* **1936**, *28*, 988–994.
- (27) van der Pauw, L. J. A method of measuring specific resistivity and Hall effect of discs of arbitrary shape. *Philips Res. Rep.* **1958**, *13*, 1–9.
- (28) Ben Belgacem, R.; Chaari, M.; Braña, A. F.; Garcia, B. J.; Matoussi, A. Structural, electric modulus and complex impedance analysis of ZnO/TiO₂ composite ceramics. *J. Am. Ceram. Soc.* **2017**, *100*, 2045–2058.
- (29) Wang, Z. L. Nanostructures of zinc oxide. *Mater. Today* **2004**, *7*, 26–33.
- (30) Arciola, C. R.; Campoccia, D.; Montanaro, L. Implant infections: adhesion, biofilm formation and immune evasion. *Nat. Rev. Microbiol.* **2018**, *16*, 397–409.
- (31) Otto, M. Staphylococcus epidermidis - the 'accidental' pathogen. *Nat. Rev. Microbiol.* **2009**, *7*, 555–567.
- (32) McCann, M. T.; Gilmore, B. F.; Gorman, S. P. Staphylococcus epidermidis device-related infections: pathogenesis and clinical management. *J. Pharm. Pharmacol.* **2008**, *60*, 1551–1571.
- (33) Zhang, L.; Ding, Y.; Povey, M.; York, D. ZnO nanofluids - A potential antibacterial agent. *Prog. Nat. Sci.: Mater. Int.* **2008**, *18*, 939–944.
- (34) Brayner, R.; Ferrari-Iliou, R.; Brivois, N.; Djediat, S.; Benedetti, M. F.; Fiévet, F. Toxicological impact studies based on Escherichia coli bacteria in ultrafine ZnO nanoparticles colloidal medium. *Nano Lett.* **2006**, *6*, 866–870.
- (35) Conrady, D. G.; Brescia, C. C.; Horii, K.; Weiss, A. A.; Hassett, D. J.; Herr, A. B. A zinc-dependent adhesion module is responsible for intercellular adhesion in staphylococcal biofilms. *Proc. Natl. Acad. Sci. U.S.A.* **2008**, *105*, 19456–19461.
- (36) Manso, M.; Ogueta, S.; García, P.; Pérez-Rigueiro, J.; Jiménez, C.; Martínez-Duart, J. M.; Langlet, M. Mechanical and in vitro testing of aerosol-gel deposited titania coatings for biocompatible applications. *Biomaterials* **2002**, *23*, 349–356.
- (37) Palacio, M. L. B.; Bhushan, B. Bioadhesion: a review of concepts and applications. *Philos. Trans. R. Soc., A* **2012**, *370*, 2321–2347.
- (38) Ben Ayadi, Z.; Mahdhi, H.; Djessas, K.; Gauffier, J. L.; El Mir, L.; Alaya, S. Sputtered Al-doped ZnO transparent conducting thin films suitable for silicon solar cells. *Thin Solid Films* **2014**, *553*, 123–126.
- (39) Woo, J.-C.; Um, D.-S.; Kim, C.-I. The dry etching of a sol-gel deposited ZnO thin film in a high density BCl₃/Ar plasma. *Thin Solid Films* **2010**, *518*, 2905–2909.
- (40) Langlet, M.; Burgos, M.; Coutier, C.; Jimenez, C.; Morant, C.; Manso, M. Low temperature preparation of high refractive index and mechanically resistant sol-gel TiO₂ films for multilayer antireflective coating applications. *J. Sol-Gel Sci. Technol.* **2001**, *22*, 139–150.
- (41) Zhang, T.; Huang, H.; Chen, R. Wet Chemical Etching Process of BST Thin Films for Pyroelectric Infrared Detectors. *Ferroelectrics* **2011**, *410*, 137–144.
- (42) Horcas, I.; Fernández, R.; Gomez-Rodriguez, J. M.; Colchero, J.; Gómez-Herrero, J.; Baro, A. M. WSXM: A software for scanning probe microscopy and a tool for nanotechnology. *Rev. Sci. Instrum.* **2007**, *78*, 013705.
- (43) Mayer, M. SIMNRA, a simulation program for the analysis of NRA, RBS and ERDA. *Application of Accelerators in Research and Industry, Pts 1 and 2*, 1999; Vol. 475, pp 541–544.
- (44) Leavitt, J. A.; McIntyre, L. C.; Stoss, P.; Oder, J. G.; Ashbaugh, M. D.; Dezfouly-Arjomandy, B.; Yang, Z. M.; Lin, Z. Cross-sections for 170.5-degrees backscattering of he-4 from carbon for he-4 energies between 1.6 and 5.0 meV. *Nucl. Instrum. Methods Phys. Res., Sect. B* **1989**, *40-41*, 776–779.
- (45) Kinnari, T. J.; Soininen, A.; Esteban, J.; Zamora, N.; Alakoski, E.; Kouri, V. P.; Lappalainen, R.; Kontinen, Y. T.; Gomez-Barrena, E.; Tiainen, V. M. Adhesion of staphylococcal and Caco-2 cells on diamond-like carbon polymer hybrid coating. *J. Biomed. Mater. Res., Part A* **2008**, *86*, 760–768.
- (46) Djurišić, A. B.; Leung, Y. H.; Ng, A. M. C.; Xu, X. Y.; Lee, P. K. H.; Degger, N.; Wu, R. S. S. Toxicity of Metal Oxide Nanoparticles: Mechanisms, Characterization, and Avoiding Experimental Artefacts. *Small* **2015**, *11*, 26–44.
- (47) Boulos, L.; Prévost, M.; Barbeau, B.; Coallier, J.; Desjardins, R. LIVE/DEAD BacLight : application of a new rapid staining method for direct enumeration of viable and total bacteria in drinking water. *J. Microbiol. Methods* **1999**, *37*, 77–86.